Supporting Information for

Activation of trace $LiNO_3$ additives by BF_3 in high-concentration electrolyte towards stable lithium metal batteries

*He-yi Xia [a], Yu-ke Wang [a], Zheng-wen Fu [a, *]*

a Shanghai Key Laboratory of Molecular Catalysis and Innovative Materials, Department of Chemistry, Fudan University, Shanghai 200433, P. R. China

*Correspondence and requests for materials should be addressed to Z.-W.F. (email: zwfu@fudan.edu.cn)

CRediT authorship contribution statement

He-Yi Xia: Conceptualization, Methodology, Investigation, Data Curation, Visualization, Writing - Original Draft. **Yu-Ke Wang:** Investigation. **Zheng-Wen Fu:** Supervision, Writing - Review & Editing, Project administration, Funding acquisition.

Acknowledgement

This work was financially supported by the National Natural Science Foundation of China (No. 22279022), the Joint Funds of the National Natural Science Foundation of China (No. U20A20336) and the Tianmu Lake Institute of Advanced Energy Storage Technologies Scientist Studio Program (No. TIES-SS0002).

Experimental Section

Electrolytes preparation. Firstly, the mass of each component is calculated according to the ratio of the amount of each component in the designed electrolyte. Considering that if the electrolyte is prepared with the concentration of the amount of substance, the change of the solution volume when the solute is dissolved is challenging to predict, especially in a high-concentration electrolyte system, so the ratio of the amount of substance is used to design the electrolyte. Then the corresponding electrolyte is prepared by weighing and mixing the related components. The specific electrolyte preparation steps are as follows: Mixing LiFSI powder and THF liquid at a mass ratio of 1: 1.16 to obtain BE electrolyte. The TN electrolyte was obtained by blending LiFSI, $LiNO_3$, and THF at a mass ratio of 1: 0.0037: 1.16. The TNB electrolyte was obtained by mixing LiFSI, $LiNO_3$, THF, and BF_3·THF at a mass ratio of 1: 0.0037: 1.15: 0.0073.

Materials characterization. Samples have been studied by X-ray Photoelectron Spectroscopy (PHI 5000 Versaprobe III) and scanning electron microscopy (Hitachi, Regulus 8100). The depth profile of XPS was performed by the source of argon ion with the etching depth of 10 nm each time, calibrated by the standard film of SiO_2.

Electrochemical measurements. Batteries were assembled in a glove box with Ar-filled (H_2O < 1 ppm; O_2 < 1 ppm). A slurry of active material ($LiFePO_4$, LFP), Super P carbon, and polyvinylidene difluoride (PVDF) mixed by 94:4:2 in the solvent of N-methyl-2-pyrrolidone (NMP) was spread on the aluminum foil as cathodes with the active mass loading of 12.0 mg cm^{-2} for the

single layer of LFP. After dried at 90 ℃ for 12 h, the foil was cut into small plates with a diameter of 12 mm. And coin cells of CR2032-type were assembled with one layer of Celgard 2325 as a separator. The volume of electrolyte added to all cells was 30 μL. The cycling tests for all cells were performed on the battery tester of Neware (LAND CT2001A). For Li/Cu half-cell CE tests, the cycling was done by depositing 1 mAh cm^{-2} of Li onto the Cu electrode at 1 mA cm^{-2}, followed by stripping to 1 V. For Li/Li symmetry cells, the cycling was done at 1 mAh cm^{-2}/2 mA cm^{-2}. The Li/LFP full cells were cycled with the following method: after the first activation cycle at 0.1 C charge/discharge, cells were cycled between 2.7 and 3.7 V at 0.5 C charge/discharge. The Li/Li symmetry cells for electrochemical impedance spectroscopy (EIS) were cycled at 1 mAh cm^{-2}/ 2 mA cm^{-2}, and after cycles, the cells rested for 2 h to test EIS. The EIS was conducted on the CHI660e electrochemical workstation. The EIS measurements were taken over a frequency range of 1 MHz to 100 mHz. For the linear sweep voltammetry measurements, Li/Cu half cells were tested over a voltage range of open-circuit voltage to 0 V at the scan rate of 0.5 mV s^{-1}. For the Tafel plots measurements, Li/Li symmetry cells were pre-cycling fifty times to form a stable interfacial layer and were tested over a voltage range of 0.2 to -0.2 V at the scan rate of 1 mV s^{-1}. The cells for XPS tests were cycled ten times at 1 mAh cm^{-2}/ 1 mA cm^{-2}, and the cells for SEM tests were cycled ten times at 1 mAh cm^{-2}/ 2 mA cm^{-2}. To be noted, the lithium sheets used for SEM tests were selected from the same side of the symmetry cells, that is, they have experienced the same electrochemical process, which can better indicate the reversibility of the lithium anodes. All batteries were tested at room temperature.

Computational methods. The optimized structure, HOMO/LUMO energies and binding energies of the anions and associated complexes (Li^+-$Anion^-$) were obtained using DFT (B3LYP) methods in the Gaussian 09 package, with the 6-311G+(d, p) basis set.[1-3] All calculations were performed under implicit solvation model with solvent of THF. The absence of imaginary frequencies is in the calculated vibrational frequencies of the optimized structures to ensure stable structures.

Three electrolyte models were constructed to model the BE, TN, and TNB electrolytes. The BE electrolyte model contains 300 THF and 100 LiFSI molecules. The TN electrolyte model contains 1500 THF, 500 LiFSI, and 5 $LiNO_3$ molecules. The TNB electrolyte model contains 1500 THF, 500LiFSI, 5 $LiNO_3$, and 5 $LiBF_4$ molecules. The reason for using $LiBF_4$ to construct the model

instead of BF_3 is due to the reaction between BF_3 and LiF to form $LiBF_4$,[4] confirmed by XPS B 1s result (Fig. S3).[5] The molecular dynamics simulations were conducted via the Forcite module in the Materials Studio of Accelrys Inc. The condensed-phase optimized molecular potentials for atomistic simulation studied (COMPASS III) force field was chosen for all the molecular dynamics simulations.[6] The electrolyte systems were equilibrated with the NPT ensemble at 298 K first, using the Berendsen algorithm to maintain the pressure of 0.1 GPa with a decay constant of 0.1 ps for 100 ps.[7] Then, the simulation that runs for 200 ps was obtained with the NVT ensemble at 298 K. The temperature was controlled by Nose algorithm.[8] The simulation time was long enough to ensure reaching the equilibrium states of the electrolyte systems. The timestep was set to be 1 fs.

Figure

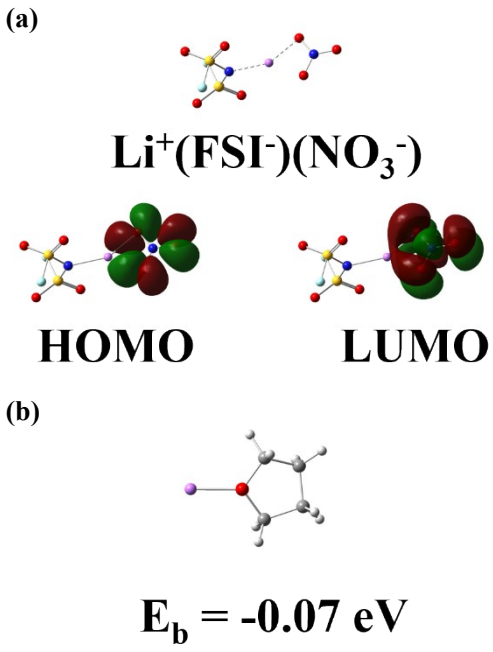

Fig. S1 (a) HOMO and LUMO of $Li^+(FSI^-)(NO_3^-)$. (b) Binding energy of Li-THF complex.

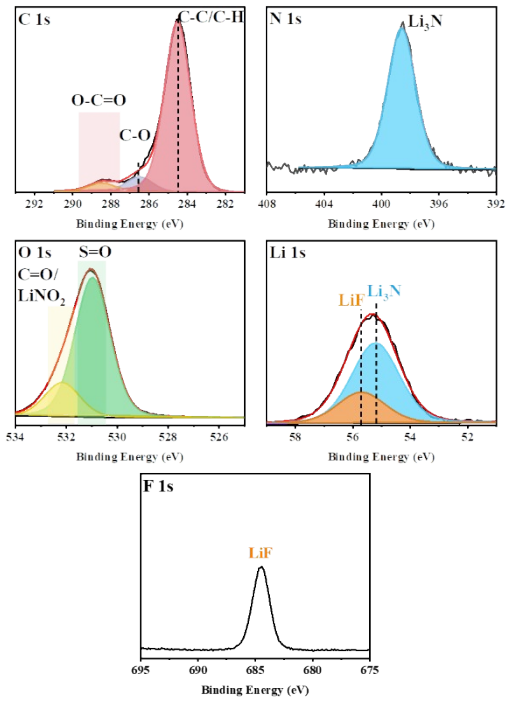

Fig. S2 XPS spectra for the surface of current collector after ten cycles in BE.

Table S1. Elemental distribution of the SEI formed on the surface of copper current collectors in different electrolytes

Elements		Li	C	N	O	F	S	B
Atomic (%)	BE	32.61	20.62	2.39	33.38	6.01	4.99	0
	TN	34.40	18.42	2.14	33.78	6.66	4.60	0
	TNB	30.30	22.72	2.22	33.14	5.68	4.44	1.50

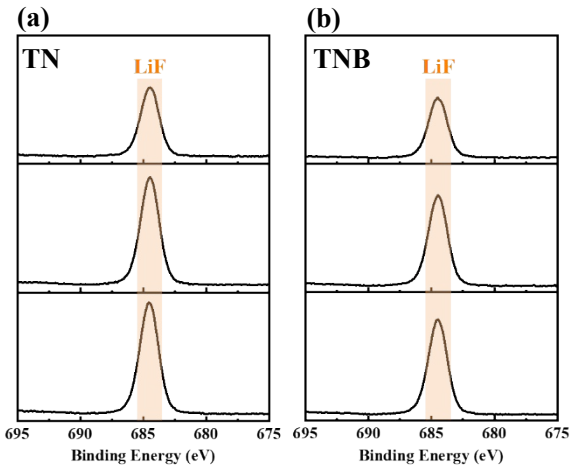

Fig. S3 XPS results (surface and double etching, about 10 nm per time) of F 1s for the surface of Cu (in Li/Cu half cells) after 10 cycles in (a) TN and (b) TNB electrolytes.

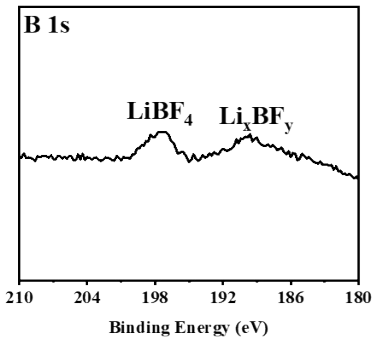

Fig. S4 XPS B 1s spectra for the surface of current collector after ten cycles in TNB.

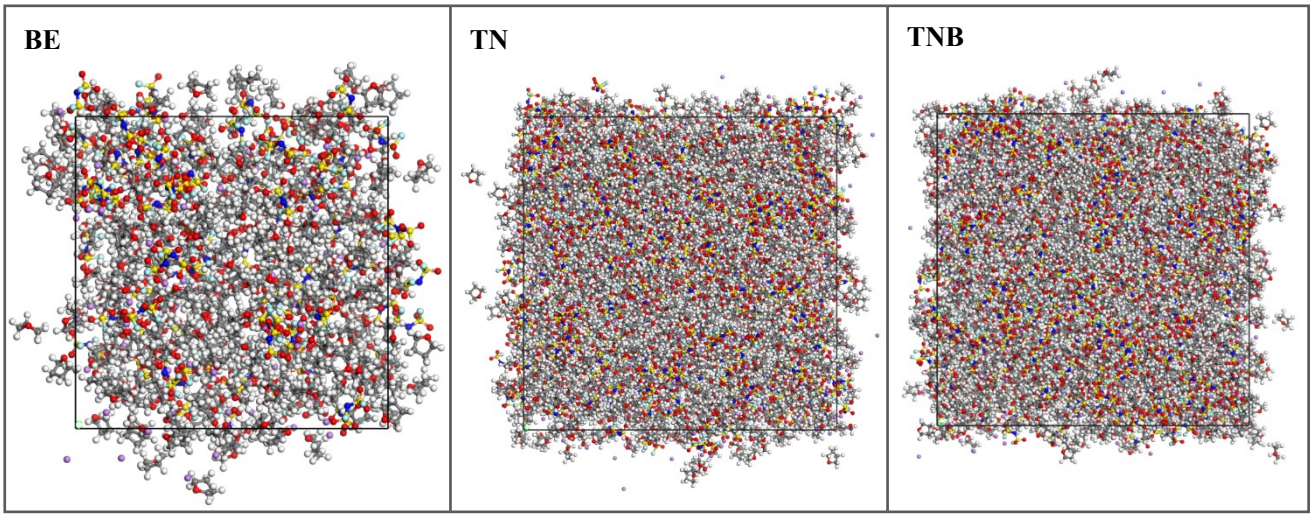

Fig. S5 Snapshots of the MD simulation boxes of BE, TN, and TNB electrolytes. Colors for different elements: oxygen, red; lithium, purple; sulfur, yellow; nitrogen, blue; carbon, gray; hidrogen, white; and fluorine, cyan.

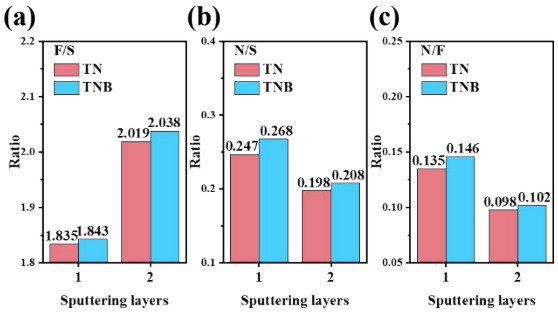

Fig. S6 (a-c) F/S, N/S, and N/F ratios of XPS spectra (after sputtering) for the surface of Cu after 10 cycles in TN and TNB electrolytes.

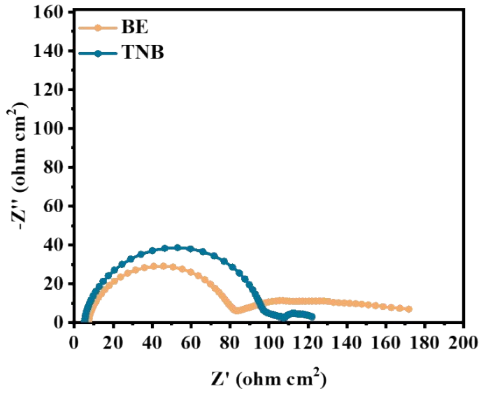

Fig. S7 EIS profiles for uncycled Li/Li cells.

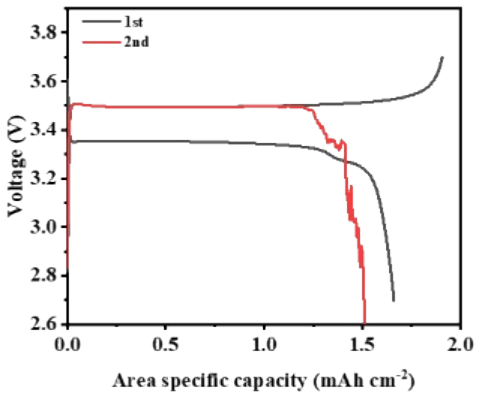

Fig. S8 Voltage profiles for Li/LFP cell in LiFSI: THF: BF_3 =1: 3: 0.01 electrolyte.

Table S2. CE and N-cotaining SEI components reported in the literatures.

Electrolyte	CE and testing condition (Li/Cu half cells)	N-containing SEI components (Derived from XPS N 1s spectra)	Ref
0.6 M LiTFSI + 0.4 M LiBOB + $LiPF_6$ in EC/EMC (4/6, v/v) + composite protective layer coating (containing 10 wt% $LiNO_3$)	/	$LiNO_3$, $LiNO_2$, Li_3N, LiN_xO_y	9
3 ml [1 M $LiPF_6$ in EC/DMC/EMC (1/1/1, v/v/v) + 5 wt% FEC + 0.1 M $LiNO_3$] + 20 mg NO_3^- -MgAl layered double hydroxides	97.3 % (0.5 mA cm^{-2}/1 mAh cm^{-2}, 300 cycles)	$LiNO_3$, $LiNO_2$, Li_3N	10
1 M $LiPF_6$ in EC/DMC (1/1, v/v) + 5 wt% FEC + 5 wt% 2.2 M $LiNO_3$ in sulfolane	99.5 % (0.5 mA cm^{-2}/0.5 mAh cm^{-2}) * (93.4 % without FEC)	$LiNO_2$, Li_3N, LiN_xO_y	11
0.6 M LiTFSI + 0.4 M LiBOB in EC/EMC (3/7, v/v) + 0.05 M $LiNO_3$	/	$LiNO_3$, $LiNO_2$, Li_3N, LiN_xO_y	12
1ml [1 M $LiPF_6$ in EC/EMC (1/1, v/v) + 2 wt% FEC] + 20.7 mg $LiNO_3$ + 180 μL tetramethylurea	97.46 % (0.5 mA cm^{-2}/1 mAh cm^{-2}, 50 cycles)	Li_3N, Li_xN_y	13
1 M $LiPF_6$ in EC/DMC/FEC (9/9/2, v/v/v) + 0.1 M $RbNO_3$ + 0.1 M 18-Crown-6	94.4 % (0.5 mA cm^{-2}/1 mAh cm^{-2}, 150 cycles)	LiN_xO_y	14
1 M $LiPF_6$ in EC/DMC (1/1, v/v) + 5 vt% FEC + 0.01 mM I_2 + 5 vt% [4 M $LiNO_3$ in tetraglyme]	98.27 % (0.5 mA cm^{-2}/1 mAh cm^{-2}, 200 cycles)	Li_3N	15
1 M $LiPF_6$ in EC/DEC (1/1, v/v) + 10 mM $In(OTf)_3$ + 0.5 M $LiNO_3$	98.1 % (1 mA cm^{-2}/1 mAh cm^{-2}, 250 cycles)	Li_3N, LiN_xO_y, R-NO_2	16

3.25 M LiTFSI in sulfolane + 0.1 M $LiNO_3$	98.5 % (0.5 mA cm^{-2}/1 mAh cm^{-2}, 100 cycles)	Li_3N, N-S	17
1 M LiFSI in FEC/γ-butyrolactone (1/2, v/v) + 0.3 M $LiNO_3$	98.4 % (0.5 mA cm^{-2}/1 mAh cm^{-2}, 200 cycles)	N-S	18
1 M LiFSI in EC + 0.5 M $LiNO_3$	98.5 % (0.5 mA cm^{-2}/1 mAh cm^{-2}, 350 cycles)	Li_3N	19
1 M $LiPF_6$ in EC/DEC (1/1, v/v) + 0.5 wt % $LiNO_3$ + 0.5 wt% CsF	98 % (1 mA cm^{-2}/1 mAh cm^{-2}, 200 cycles)	Li_3N, LiN_xO_y	20
2M LiFSI in DME + 2 M $LiNO_3$	98.5 % (1 mA cm^{-2}/1 mAh cm^{-2}, 250 cycles)	R-NO_2, LiTFSI, N-SO_x, Li_3N	21
1 M $LiPF_6$ in FEC/EMC (3/7, v/v) + 2 wt% $LiBF_4$ + 2 wt% $LiNO_3$	98.5 % (1 mA cm^{-2}/1 mAh cm^{-2}, 250 cycles)	$LiNO_3$, Li_3N, LiN_xO_y	22
1 M LiTFSI in DOL/DME (1/1, v/v) + 2 wt% $LiNO_3$ + 0.2 M thiourea	97.69 % (1 mA cm^{-2}/1 mAh cm^{-2}, 200 cycles)	NSO_2^-, Li_3N	23
TNB	98.82 % (1 mA cm^{-2}/1 mAh cm^{-2}, 200 cycles)	Li_3N, LiN_xO_y	Our work

*CE was tested via the Zhang's method 3,[24] otherwise by the same half-cell test way as ours.

1. R. Peverati and D. G. Truhlar, *The Journal of Physical Chemistry Letters*, 2011, **3**, 117-124.
2. A. Austin, G. A. Petersson, M. J. Frisch, F. J. Dobek, G. Scalmani and K. Throssell, *J Chem Theory Comput*, 2012, **8**, 4989-5007.
3. S. V. Sambasivarao and O. Acevedo, *Journal of chemical theory and computation*, 2009, **5**, 1038-1050.
4. Q. Li, W. Xue, X. Sun, X. Yu, H. Li and L. Chen, *Energy Storage Materials*, 2021, **38**, 482-488.
5. B. S. Parimalam and B. L. Lucht, *Journal of The Electrochemical Society*, 2018, **165**, A251-A255.
6. R. L. C. Akkermans, N. A. Spenley and S. H. Robertson, *Molecular Simulation*, 2020, **47**, 540-551.
7. H. J. C. Berendsen, J. P. M. Postma, W. F. van Gunsteren, A. DiNola and J. R. Haak, *The Journal of Chemical Physics*, 1984, **81**, 3684-3690.
8. S. Nosé, *Molecular Physics*, 2006, **52**, 255-268.
9. J.-T. Kim, I. Phiri and S.-Y. Ryou, *ACS Applied Energy Materials*, 2023, **6**, 2311-2319.
10. F. Wang, Z. Wen, Z. Zheng, W. Fang, L. Chen, F. Chen, N. Zhang, X. Liu, R. Ma and G. Chen, *Advanced Energy Materials*, 2023, **13**.
11. N. Piao, S. Liu, B. Zhang, X. Ji, X. Fan, L. Wang, P.-F. Wang, T. Jin, S.-C. Liou, H. Yang, J. Jiang, K. Xu, M. A. Schroeder, X. He and C. Wang, *ACS Energy Letters*, 2021, **6**, 1839-1848.
12. I. Phiri, J. Kim, D. H. Oh, M. Ravi, H. S. Bae, J. Hong, S. Kim, Y. C. Jeong, Y. M. Lee, Y. G. Lee and M. H. Ryou, *ACS Appl Mater Interfaces*, 2021, **13**, 31605-31613.
13. Z. Piao, P. Xiao, R. Luo, J. Ma, R. Gao, C. Li, J. Tan, K. Yu, G. Zhou and H. M. Cheng, *Adv Mater*, 2022, **34**, e2108400.
14. S. Gu, S. W. Zhang, J. Han, Y. Deng, C. Luo, G. Zhou, Y. He, G. Wei, F. Kang, W. Lv and Q. H. Yang, *Advanced Functional Materials*, 2021, **31**.
15. Z. Wen, W. Fang, X. Wu, Z. Qin, H. Kang, L. Chen, N. Zhang, X. Liu and G. Chen, *Advanced Functional Materials*, 2022, **32**.
16. W. Zhang, Z. Shen, S. Li, L. Fan, X. Wang, F. Chen, X. Zang, T. Wu, F. Ma and Y. Lu, *Advanced Functional Materials*, 2020, **30**.
17. J. Fu, X. Ji, J. Chen, L. Chen, X. Fan, D. Mu and C. Wang, *Angew Chem Int Ed Engl*, 2020, **59**, 22194-22201.
18. Y. Jie, X. Liu, Z. Lei, S. Wang, Y. Chen, F. Huang, R. Cao, G. Zhang and S. Jiao, *Angew Chem Int Ed Engl*, 2020, **59**, 3505-3510.
19. Q. Zhao, N. W. Utomo, A. L. Kocen, S. Jin, Y. Deng, V. X. Zhu, S. Moganty, G. W. Coates and L. A. Archer, *Angew Chem Int Ed Engl*, 2022, **61**, e202116214.
20. J. Zhao, Z. Wan, X. Zeng, M. Tian, K. Wang, X. Chen, M. Ling, W. Ni and C. Liang, *Inorganic Chemistry Frontiers*, 2023, **10**, 1809-1817.
21. D. W. Kang, J. Moon, H.-Y. Choi, H.-C. Shin and B. G. Kim, *Journal of Power Sources*, 2021, **490**.
22. X. Wang, S. Li, W. Zhang, D. Wang, Z. Shen, J. Zheng, H. L. Zhuang, Y. He and Y. Lu, *Nano Energy*, 2021, **89**.
23. S. Kim, K. Y. Cho, J. Kwon, K. Sim, D. Seok, H. Tak, J. Jo and K. Eom, *Small*, 2023, DOI: 10.1002/smll.202207222, e2207222.
24. B. D. Adams, J. Zheng, X. Ren, W. Xu and J. G. Zhang, *Advanced Energy Materials*, 2017, **8**.